Femtosecond Fluorescence Dynamics of Rotation-Restricted Azobenzenophanes: New Evidence on the Mechanism of *trans* → *cis* Photoisomerization of Azobenzene

Ying-Chih Lu and Eric Wei-Guang Diau*

Department of Applied Chemistry, Institute of Molecular Science, and
Center for Interdisciplinary Molecular Science, National Chiao Tung University, Hsinchu 30010, Taiwan

Hermann Rau

FG Physikalische Chemie, Institute für Chemie, Universität Hohenheim, D-7000 Stuttgart 70, Germany
Received: November 5, 2004; In Final Form: December 26, 2004

The ultrafast relaxation dynamics of two rotation-restricted (azobenzeno-2*S*-phane and azobenzeno-4*S*-phane) and one rotation-free (4,4′-dimethylazobenzene) azobenzene derivatives were investigated using femtosecond fluorescence up-conversion on both $S_1(n,\pi^*)$ and $S_2(\pi,\pi^*)$ excitations. On S_2 excitation, pulse-limited kinetics with a decay coefficient of ∼100 fs corresponding to ultrafast $S_2 \rightarrow S_1$ relaxation is found to be common for all molecules under investigation regardless of the molecular structure. This indicates that a direct rotational relaxation on the S_2 surface is unfavorable. On S_1 excitation, we observed biphasic fluorescence decay with a femtosecond component attributed to the decay of the Franck−Condon state prepared by excitation and a picosecond component attributed to the deactivation of the relaxed molecule on the S_1 surface. This picosecond component is slowed by at least a factor of 2 for the rotation-restricted 2*S*-bridged molecule compared to that of the rotation-free molecule; for the even stronger rotation-restricted azobenzeno-4*S*-phane, the decrease is by a factor of 10. These differences in deactivation suggest that the relaxed states and probably the trajectories for rotation-free and rotation-restricted molecules are different on the S_1 surface, which should be important for the quantum yield of photoisomerization.

1. Introduction

Azobenzene is the most widely used element in photoresponsive systems and devices.[1] The function of these is based on the geometrical isomerization of the azobenzene element and its photostability. Recently, there has been a protracted debate about the mechanism of *trans* → *cis* photoisomerization of *trans*-azobenzene (AB),[2−7] whether it proceeds through an out-of-plane rotation about the N≡N double bond (*rotation mechanism*) or an in-plane inversion of the angle at the azo-nitrogen atoms. Calculations for the ground-state thermal isomerization of AB indicated that the asymmetric inversion at only one nitrogen atom (*inversion mechanism*) is energetically much more favorable than the symmetric inversion of two nitrogen atoms simultaneously (*concerted inversion mechanism*), and the former mechanism was generally accepted for excited-state isomerization as well.[2] Only recently, the latter mechanism has been reintroduced to the debate.[7]

On the basis of steady-state measurements of the quantum yield (Φ) for the *trans* → *cis* photoisomerization of AB (Φ of AB is ∼0.25 on S_1 excitation but it decreases to ∼0.1 on S_2 excitation; however, Φ is almost identical (∼0.25) on both excitations when the rotation channel is blocked in azobenzene derivatives via chemical modifications)[8−11] and on early theoretical work,[12] the conclusion (Rau's hypothesis) was drawn that the mechanism of photoisomerization of AB should differ for S_1 and S_2 excitations, namely, inversion in the S_1 state and rotation in the S_2 state, respectively. This conclusion was widely adopted after recent femtosecond spectral investigations of AB and its derivatives.[13−18]

Rau's hypothesis was first modified by Tahara and co-workers[4] on the basis of a series of real-time observations summarized below. Temporally resolved Raman measurements[19] on S_2 excitation show great similarity of S_1 and S_0 Raman spectra so that the observed S_1 transient species has a planar structure about the N≡N bond, a feature that is consistent with Rau's proposal for an inversion mechanism operating in the S_1 state. Subsequent femtosecond fluorescence experiments[20] indicated the quantum yield for the $S_2 \rightarrow S_1$ transition to be essentially unity, from which one infers that isomerization in the S_2 state is unimportant, but that isomerization of AB takes place exclusively in the S_1 state, by inversion, regardless of the initial excitation. This is in dissent with Rau's dual mechanism. To rationalize the wavelength dependence of the isomerization quantum yields, a new relaxation channel (*rotational deactivation*) has been proposed that becomes open in the vibrationally hot S_1 state of AB, forming only the trans isomer. Even though the photoisomerization mechanism of AB in the S_2 state differs between Rau's and Tahara's hypotheses, isomerization in the S_1 state via the inversion channel is a conclusion common to both models.

Many advanced theoretical investigations of the isolated AB molecule on this controversial topic have been conducted.[6,7,21−24] The most important feature found thereby is that the S_1 potential-energy surface (PES) of AB involves a substantial energy barrier along the CNN bending coordinate (*inversion channel*), whereas the surface is almost barrierless along the CNNC torsional coordinate (*rotation channel*). Indeed, early experiments have shown a very small temperature dependence of the *trans* → *cis* isomerization with an activation energy of 1−2 kJ mol⁻¹.[25] Furthermore, the lowest conical intersection (CI) between the

* Author to whom correspondence should be addressed. Fax: (886)-03-572-3764. E-mail: diau@mail.ac.nctu.edu.tw.

Femtosecond Dynamics of Azobenzenophanes

J. Phys. Chem. A, Vol. 109, No. 10, 2005 **2091**

S_0 and S_1 states was found to be located near the midpoint of the rotational pathway, indicating that photoisomerization of AB on the S_1 PES might favor a rotational mechanism.[6,7,22,24] The wavelength dependence of the isomerization quantum yields was explained in a trajectory simulation based on a semiclassical surface-hopping approach to be a purely dynamical effect.[6] In that wave packet dynamics work, Φ values on S_2 and S_1 excitations differ because of a competition between the $S_1 \rightarrow S_0$ internal conversion (IC) and the torsional motion about the N=N bond. On S_2 excitation, after fast $S_2 \rightarrow S_1$ conversion, an early $S_1 \rightarrow S_0$ IC condition with a larger CNNC torsional angle was attained on the S_1 surface, leading to a more decreased Φ than that on direct S_1 excitation. The simulated results[6] also indicate that the most effective motion to promote the $S_1 \rightarrow S_0$ IC is a symmetric opening of the two CNN bending angles, which corresponds to the concerted inversion channel.[7] It is mainly the larger amplitude of this symmetric CNN bending motion that allows the molecule to approach the S_0–S_1 crossing seam along the rotation channel, thus favoring the early IC. Hence, high-level calculations predict that only the rotational mechanism operates, incorporating a symmetric CNN bending motion, for photoisomerization of AB in the S_1 state irrespective of initial excitation. This is in disagreement with Rau's and Tahara's hypotheses.

Experimental evidence supporting the rotational mechanism is provided from femtosecond fluorescence anisotropy measurements of AB on direct S_1 excitation.[26] The observed S_1 fluorescence depolarization of AB in hexane is highly anisotropic, with the rotational time coefficient (1–2 ps) the same as that of the slow component of the transient fluorescence decay in hexane; in contrast, the anisotropies are nearly constant during the corresponding decays in a viscous solvent such as ethylene glycol (EG). Therefore, photoisomerization of AB in the S_1 state was proposed to occur through the rotational channel in hexane, but another mechanism should be considered when the rotational motion is substantially hindered in EG, presumably concerted inversion. Similarly, such a solvent dependence on S_1 lifetime of AB in the same solvents is reported from the time-resolved Raman experiments of Tahara and co-workers;[4,19] the decay coefficient is as small as ~1 ps in hexane but increases to ~12.5 ps in EG. As pointed out elsewhere,[26] the observed planar S_1 species in transient Raman spectra cannot exclude subsequent $S_1 \rightarrow S_0$ photoisomerization through the rotational channel because the twisted S_1 species might be either Raman inactive or too transient to be observed. We thus conjecture that two distinct mechanisms of isomerization are involved in the S_1 state that become dominant in different solvents with disparate viscosity as proposed from the femtosecond fluorescence anisotropy work;[26] the rotation mechanism operates in a nonviscous solvent, the concerted inversion mechanism probably prevails when the rotation channel is obstructed in a viscous solvent, and the *trans* → *cis* isomerization would occur exclusively on the ground-state surface.[26]

According to femtosecond time-resolved absorption spectra[14,15,18,27] and fluorescence up-conversion[26,28] measurements of AB on S_1 excitation, the transient species in nonviscous solvents feature two decay components with rapid and slow components decaying on time scales 100–300 fs and 1–3 ps, respectively. The femtosecond component is accepted to be due to the motion of the excited-state molecule out of the Franck–Condon (FC) region on the S_1 PES, whereas the picosecond component corresponds to a subsequent motion searching for the S_0/S_1 CI, presumably along the rotation channel according to theoretical investigations.[6,7] Rotational isomerization of AB

CHART 1: Chemical Structures of DMAB, 2S-ABP, and 4S-ABP
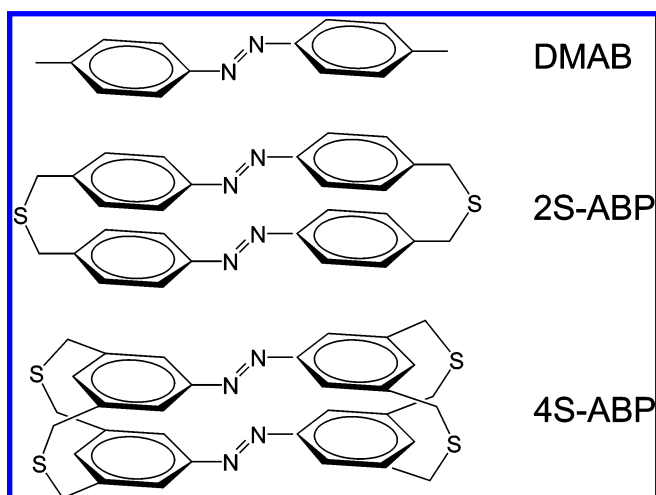
is, however, unfeasible for a rotation-restricted AB derivative, whereby large-scale motion of phenyl groups is substantially constrained via chemical modification.[8,9] One example was given by ultrafast time-resolved absorption spectral measurements;[16] the observed lifetimes upon S_2 excitation are ~1 ps and ~2.6 ps for AB and AB capped with an azacrown ether in chloroform, respectively. This evident discrepancy observed in lifetimes between the two molecules indicates that the restricted rotational freedom of the phenyl groups in the capped AB has a significant effect on excited-state dynamics and the photo-isomerization mechanism of AB but the results were interpreted according to the conventional dual mechanism model.

In this paper, we report femtosecond fluorescence dynamics of two rotation-restricted azobenzenophanes, 19-dithia[3.3](4,4')-*trans*-diphenyldiazeno-2-phane (2*S*-ABP) and 2,19,36,39-tetrathia[3.3.3.3](3,3',5,5')-*trans*-diphenyldiazeno-4-phane (4*S*-ABP), for which the out-of-plane rotational motion is significantly restricted in both molecules. The rotation-free azo molecules, AB and 4,4'-dimethyl *trans*-azobenzene (DMAB), were also studied in nonviscous solvents for comparison. The chemical structures of DMAB, 2*S*-ABP, and 4*S*-ABP are shown in Chart 1. From earlier experiments,[9,11] we know that the isomerization process occurs sequentially in the phanes and that the exciton interaction has no decisive effect on their photochemistry. So we can infer that our experiments reflect the initial steps of the photoinduced isomerization of an azobenzene unit in DMAB, 2*S*-ABP, and 4*S*-ABP. The prominent dynamical effect on molecular rigidity observed might provide important information to resolve the enduring controversy about the mechanism of the photoisomerization of azobenzene.

2. Experimental Section

2.1. Femtosecond Fluorescence Up-Conversion Setup. Femtosecond time-resolved fluorescence measurements were performed using an integrated fluorescence up-conversion system (FOG100, CDP) in combination with a mode-locked Ti:sapphire laser (Mira 900D, Coherent) pumped with a 10 W Nd:YVO$_4$ laser (Verdi-V10, Coherent). The experimental setup is shown in Figure 1. In principle, the system is similar to that reported previously,[28] but a minor modification was made to improve the signal-to-noise ratio through collecting the emission using two parabolic mirrors instead two lenses. The output of the laser pulse was tuned in the wavelength range 720–960 nm with an average power 0.6–1.7 W. The spectral profile of the pulse was measured with an ultrafast laser-spectrum analyzer
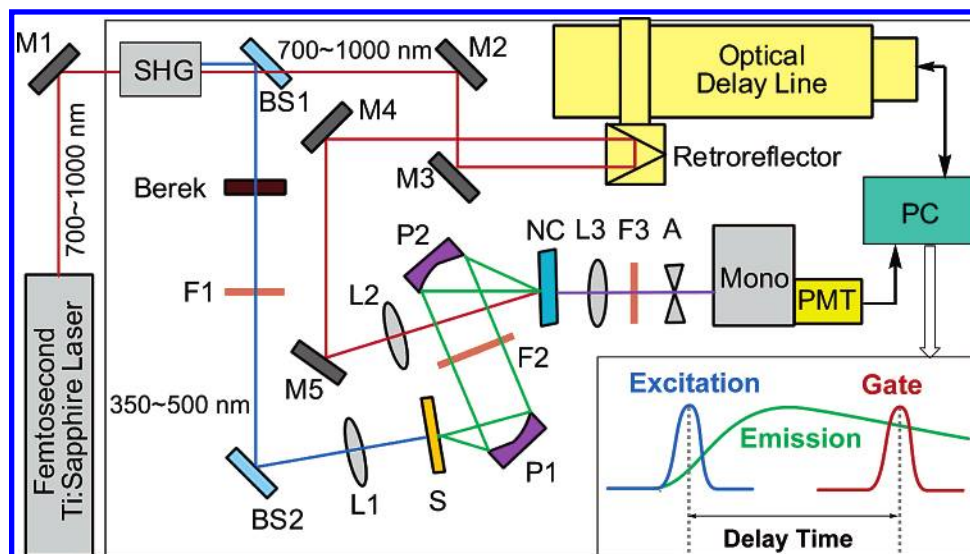
Figure 1. Femtosecond fluorescence up-conversion spectrometer. A, aperture or iris; BS1−BS2, beam splitters; F1−F3, color filters; L1−L3, focusing lenses; M1−M5, broadband dielectric mirrors; Mono, double monochromator; NC, nonlinear crystal; P1−P2, parabolic mirrors; PC, personal computer; S, rotary sample cell; PMT, photomultiplier tube; SHG, optical set for second-harmonic generation.

(E201, REES); the profile in a typical spectrum has a full width at half-maximum (fwhm) intensity in the range of 8−12 nm. The pulse duration was determined with an autocorrelator (Mini, APE), with a typical fwhm of autocorrelation of the pulse measured to be ∼140 and ∼220 fs at 860 and 720 nm, respectively.

The femtosecond pulses were focused onto a LBO type-I nonlinear crystal (thickness 0.8 mm) for second-harmonic generation (SHG) to produce excitation pulses in the range of 360−480 nm. Excitation pulses were separated from fundamental pulses with a dichroic beam splitter (BS1) and used as pump pulses; these pump pulses were then focused to a diameter of ∼100 μm onto a rotating cell (S, thickness 1 mm) containing a sample solution with a volume of ∼0.7 cm^3. The energy of the pump beam was attenuated to be less than 1 nJ/pulse in order to avoid irreversible photoreactions. The fluorescence emitted from the sample was collected with two parabolic mirrors (P1 and P2) and focused onto a BBO type-I crystal (NC, thickness 0.5 mm). The optically delayed fundamental pulses were also focused on the NC and served as gate pulses for sum-frequency generation (SFG). The energy of the gate pulse was kept as high as possible, e.g., typical energy was ∼7 nJ/pulse at 860 nm. The SFG signal was spatially and spectrally separated from other interfering light with an iris (A), an appropriate interference filter (F3), and a double monochromator (DH10, Jobin-Yvon) in combination. The signal was detected with a photon-counting photomultiplier tube (PMT, R1527P, Hamamatsu) and transferred to a computer through an RS-232 interface for data acquisition and manipulation. A Berek variable wave plate placed in the optical path of the excitation pulse was carefully adjusted to ensure that the polarization between the excitation and the probe pulses is at the magic-angle (54.7°) configuration. As illustrated in the inset of Figure 1, the transient profile of the emission is obtained by varying the delay between the excitation and the gate pulses through the optical delay line.

2.2. Data Analysis and Kinetic Model. The transient signal, $I(t)$, was fitted by a convolution of the instrument response function $g(t)$ with an appropriate kinetic function $f(t)$[29]

$$I(t) = \int_0^\infty g(t - s)f(s) \, \mathrm{d}s \quad (1)$$

where $g(t)$ is normally a Gaussian function and $f(t)$ is the

molecular response function; the choice of a $f(t)$ relies on a proper kinetic model (see below). Two important parameters, time zero and instrument response function, should be precisely determined in order to extract the kinetics (in particular with the fast-decay component of which the lifetime is comparable to the fwhm of the laser pulse) from deconvolution.[29,30] Both time zero and the fwhm of $g(t)$ were treated as free parameters in our nonlinear curve fitting procedure because these two parameters strongly depend on the probing wavelength due to the group velocity dispersion (GVD) detailed elsewhere.[28]

The temporal characteristic of the pulse (instrument response function) at the excitation wavelength (λ_{ex}) can be estimated from the temporal profile of the third-harmonic generation (THG) signal obtained from SFG of the excitation and the gate pulses. When the wavelength of the probe window was tuned to the region where the fluorescence signal (at the wavelength λ_{fl}) can be effectively up-converted (presumably the phase-matching criterion is satisfied), the transients for the photo-isomerization dynamics of the azo compounds under investigation were collected. In the present study, a simple consecutive kinetic model is employed to account for the observed temporal profiles

$$A \xrightarrow{\tau_1} B \xrightarrow{\tau_2} C \quad (2)$$

where the component A is described by a single-exponential function with a decay time coefficient τ_1 and the component B is described by a biexponential function with a rise time coefficient τ_1 and a decay time coefficient τ_2. That is to say that the kinetic response function $f(t)$ is expressed as

$$f(t) = a \exp\left(-\frac{t}{\tau_1}\right) + b\left[\exp\left(-\frac{t}{\tau_2}\right) - \exp\left(-\frac{t}{\tau_1}\right)\right] \quad (3)$$

where the preexponential factors a and b represent the relative weights (or amplitudes) for components A and B, respectively.

2.3. Sample Preparation and Experimental Conditions. 2S-ABP and 4S-ABP were prepared and purified according to literature procedures;[8] AB and DMAB (Aldrich, 99% and >95%) were used without further purification. Both 2S-ABP and 4S-ABP molecules are very poorly soluble in most solvents because of their perfectly packed structure in the crystal; only
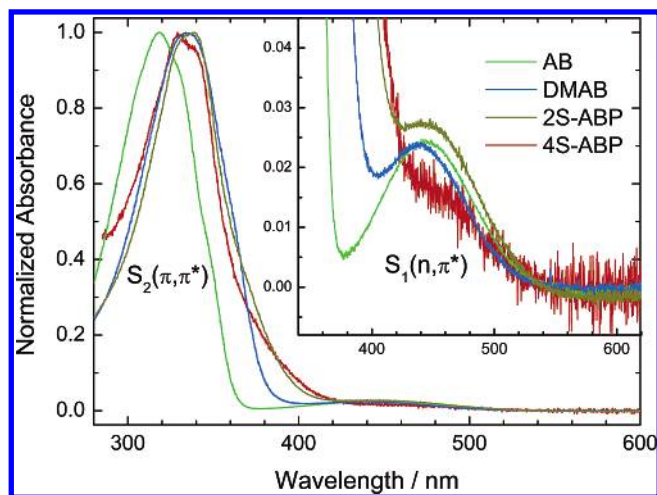
Femtosecond Dynamics of Azobenzenophanes

J. Phys. Chem. A, Vol. 109, No. 10, 2005 **2093**

Figure 2. Absorption spectra of AB, DMAB, 2*S*-ABP, and 4*S*-ABP. All samples are dissolved in CH_2Cl_2 except 4*S*-ABP in benzene. The absorbance of each spectrum is normalized at the maximum of the S_2 band for comparison; an inset shows spectra enlarged in the region of S_1 absorption.

TABLE 1: Summary of Fitted Time Coefficients of 2*S*-ABP at Various Excitation and Fluorescence Wavelengths[a]

λ_{ex}/nm	λ_{fl}/nm	fwhm[b]/fs	τ_1/fs	τ_2/ps
360	450	270	110 (1.00)	
	500	280	100 (0.98)	
	550	230	110 (0.89)	2.5 (0.10)
380	600	260	160 (0.83)	3.2 (0.15)
400	500	210	60 (0.98)	1.5 (0.02)
	550	210	90 (0.93)	1.3 (0.06)
	600	210	190 (0.84)	3.1 (0.14)
	650	220	260 (0.77)	5.9 (0.21)
430	700	200	480 (0.74)	5.7 (0.26)
440	550	290	110 (0.91)	1.4 (0.09)
	600	250	340 (0.81)	3.5 (0.18)
	650	270	500 (0.77)	5.5 (0.23)
	700	290	590 (0.72)	6.0 (0.27)
480	600	230	240 (0.82)	2.9 (0.17)

[a] Relative weights are given in parentheses; an offset is involved for the sum of the weights less than 1.00. [b] Values are the full width at half-maximum of the instrument response function obtained from the fit.

TABLE 2: Comparison of Fitted Time Coefficients for DMAB and 4*S*-ABP at Various Excitation and Fluorescence Wavelengths[a]

		DMAB		4*S*-ABP	
λ_{ex}/nm	λ_{fl}/nm	τ_1/fs	τ_2/ps	τ_1/fs	τ_2/ps
360	450	80 (1.00)		100 (1.00)	
	500	70 (0.97)	0.9 (0.03)	120 (0.97)	4.1 (0.03)
	550	80 (0.87)	0.9 (0.13)		
	600	90 (0.70)	1.1 (0.30)		
430	550	270 (0.82)	1.8 (0.18)	70 (0.97)	1.3 (0.02)
	600	290 (0.77)	2.0 (0.23)	130 (0.86)	5.9 (0.12)
	650	360 (0.75)	2.4 (0.25)	590 (0.67)	14.1 (0.26)
	700	340 (0.71)	2.5 (0.29)	2600 (0.66)	56.2 (0.30)

[a] Relative weights are given in parentheses; an offset is involved for the sum of the weights less than 1.00.

polarizable solvents dissolve low concentrations slowly. For this reason, a solution was prepared by dissolving a sample in a polarizable solvent and shaking in a timing supersonic vessel for several days before the experiments. 2*S*-ABP was partially dissolved in CH_2Cl_2 (Merck, pro analysi) to the saturated concentration $\sim 1 \times 10^{-4}$ M. 4*S*-ABP is essentially insoluble in CH_2Cl_2 but dissolved slightly in benzene (Merck, pro analysi); the concentration for time-resolved measurements was estimated to be $\sim 2 \times 10^{-5}$ M. The partially dissolved solutions were filtered through a membrane filter (size < 200 nm) before use in order to eliminate undissolved particles in the solutions.[31] The sample concentrations of AB and DMAB were 5×10^{-3} and 1×10^{-3} M, respectively. All measurements were performed at ambient temperature (23 ± 1 °C).

It has been recognized that irreversible photoreactions of the azobenzenophanes could occur by prolonged irradiation of the sample solutions at 313 nm.[8] However, our measurements were performed at much longer wavelengths and low laser intensities, which do not cause two-photon absorption. Under such experimental conditions, the effect of the irreversible photoreactions on our results is negligible for the following two points. First, the fluorescence transients of the sample solutions were collected repeatedly for many times (depending on the overall signal-to-noise ratio of the transients), and the maximum signal level of each scan has been checked to be almost identical. Second, rotation of the sample cell would certainly help to avoid the accumulation of isomerized or decomposed compounds. In addition, fresh sample solutions were used for each set of the experiments, and UV−vis absorption spectra of the solutions were checked to be almost identical before and after the laser experiments. Therefore, the possibility of a bond-breaking of the CH_2-S-CH_2 bridge occurring in either 2*S*-ABP or 4*S*-ABP is expected to be negligible under our experimental conditions.

3. Results and Discussion

Steady-state UV−vis absorption spectra of 2*S*-ABP, 4*S*-ABP, DMAB, and AB are shown in Figure 2. Absorption spectra of both 2*S*- and 4*S*-bridged azobenzenophanes feature a weak symmetry-forbidden $S_1(n,\pi^*)$ band and a strong symmetry-allowed $S_2(\pi,\pi^*)$ band, like AB and DMAB, but there is an additional absorption at approximately 380 nm in both 2*S*-ABP and 4*S*-ABP spectra that might be due to the S_2-S_2 exciton

coupling of the two azobenzene units. The $\pi \rightarrow \pi^*$ transition is significantly red-shifted in spectra of DMAB, 2*S*-ABP, and 4*S*-ABP by comparison with the spectrum of AB, whereas the $n \rightarrow \pi^*$ transition position is virtually the same in all spectra. Figure 2 also indicates that DMAB is a better spectroscopic match to the phanes than AB.

No emission is observed for any of the azo compounds under investigation using a conventional steady-state spectrofluorometer because of their extremely low fluorescence quantum yields.[20] However, the fluorescent emissions of the azo molecules have been successfully observed in the picosecond time scale using our femtosecond up-conversion spectrometer. As a result, we measured femtosecond fluorescence dynamics of 2*S*-ABP in CH_2Cl_2 on both S_1 and S_2 excitations (λ_{ex} = 360−480 nm) in a broad fluorescence spectral range (λ_{fl} = 450−700 nm);[32] the results are summarized in Table 1. For comparison, the experiments were performed at λ_{ex} = 360 nm and λ_{ex} = 430 nm for both DMAB (in CH_2Cl_2) and 4*S*-ABP (in benzene); the results are summarized in Table 2. Detailed analysis and discussion for the observed excited-state dynamics follow.

3.1. 2*S*-ABP. *3.1.1. S_1 Dynamics and Kinetic Model.* We extensively investigated the dynamics of the rotation-restricted azobenzenophane in the S_1 state by exciting 2*S*-ABP in CH_2-Cl_2 at λ_{ex} = 440 nm. There might be a little contribution from the S_2 excitation, but the similarity of the data in the range of $S_1 \rightarrow S_0$ emission regardless of excitation wavelength suggests
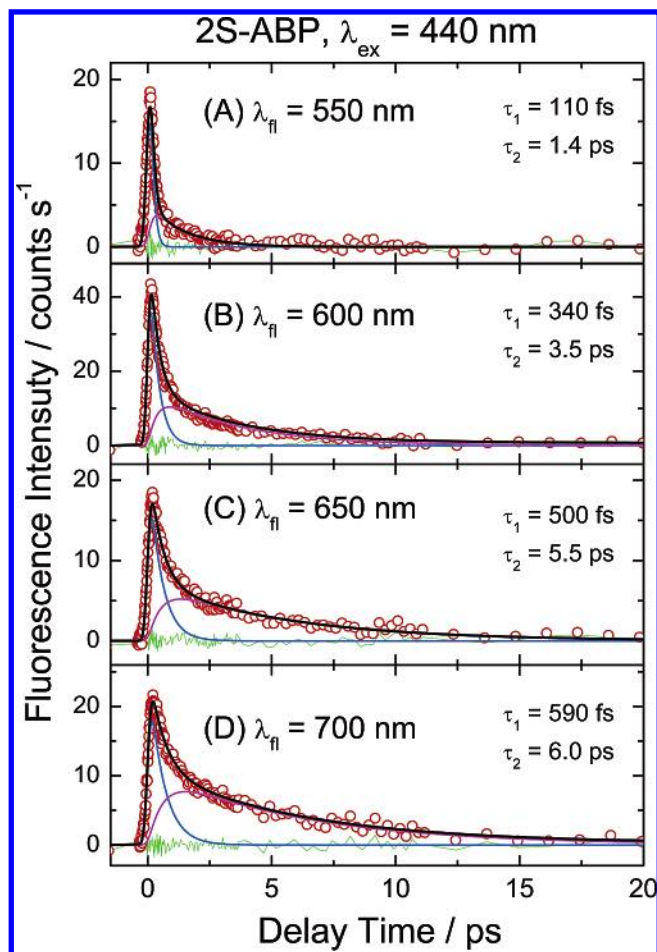
Figure 3. Femtosecond fluorescence transients of 2*S*-ABP obtained at λ_{ex} = 440 nm with fluorescence probed at λ_{fl} (nm) = (A) 550, (B) 600, (C) 650, and (D) 700. The transients were fitted according to a simple consecutive model (eqs 2 and 3) with convolution of the laser pulse (eq 1). Open circles denote raw data; solid black curves represent theoretical fits with residues shown as green traces; the blue and magenta curves under each transient are deconvoluted components corresponding to A and B (in eq 2), respectively.

that the results are essentially due to the properties of the S_1 state. The results shown in Figure 3 in four parts, from top to bottom, are the fluorescence transients observed at λ_{fl} = 550, 600, 650, and 700 nm, respectively. All transients show a biphasic dynamical feature characterized by two decay components. We infer the observed S_1 dynamics in 2*S*-ABP to reflect the involvement of two dynamical processes: (i) an initial nuclear relaxation from the Franck–Condon (FC) region to the S_1 minimum area producing the fast-decay component; (ii) the subsequent key motion(s) from the S_1 minimum toward the photochemical funnel area for electronic relaxation producing the slow-decay component. A consecutive kinetic model (eq 2) is thus proposed to describe the fluorescence transients with convolution of the laser pulse according to eq 1. In eq 2, we assume that A represents the initial FC state upon excitation, B denotes the "relaxed" state on the $S_1(n,\pi^*)$ surface (the S_1 minimum), and C denotes the photochemical funnel between the S_1 and the S_0 states (S_0/S_1 CI). Hence, the excited 2*S*-ABP decays with a time coefficient τ_1 from the FC state to the S_1 minimum and then from this minimum searches for the S_0/S_1 CI with a decay coefficient τ_2; eq 3 quantitatively describes the observed kinetics.

According to calculations of the excited state of azobenzene, a planar local minimum on the S_1 PES is attainable along the concerted inversion channel in which both in-plane symmetrical

SCHEME 1: A Cascade Dynamical Relaxation Model for 2*S*-ABP and 4*S*-ABP
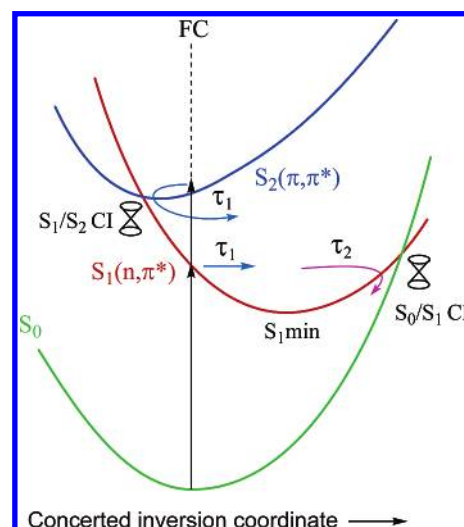
CN stretching and CNN bending motions are involved.[6,7] Further progress along this coordinate leads to a sloped S_0/S_1 CI at the molecular geometry near a linear CNNC conformation at higher energy.[7] The energetically most favorable electronic relaxation pathway in AB proceeds notably through the rotation channel with a S_0/S_1 CI near the 90° twisted molecular geometry.[6,7] The detailed shapes of the PES at the CIs are the dominant determinants for the ratio of *trans*- and *cis*-isomer formed.

For the relatively rigid 2*S*-ABP, the PES will be modified, and although the observed biphasic dynamical feature of 2*S*-ABP is similar to that of the free AB molecule, this need not indicate the same trajectories on the S_1 PES. Indeed, for the rotation-restricted 2*S*-ABP, we expect the involvement of a nonrotational motion. On the basis of recent theoretical calculations of AB,[6,7] we propose that this relaxation channel in 2*S*-ABP is related to the concerted inversion motion reaching finally a S_0/S_1 CI and thus yielding efficient $S_1 \rightarrow S_0$ internal conversion observed as the slow-decay component in the fluorescence transients. A cascade dynamical model based on theoretical calculations of AB is shown in Scheme 1 to illustrate the observed dynamical behavior (on both S_1 and S_2 excitations) for the rotation-restricted species, 2*S*-ABP.

3.1.2. Dependency on Fluorescence Wavelength. Our results of 2*S*-ABP shown in Figure 3 indicate that both τ_1 and τ_2 systematically increase as a function of λ_{fl} with the relative amplitude of the former being much larger than that of the latter at smaller λ_{fl} (i.e., the contribution of the latter becomes more significant at greater λ_{fl}). We have demonstrated in work on AB that the detection window is broad at large λ_{fl} but narrow at small λ_{fl}.[28] This broad detection at large λ_{fl} would probe more partially relaxed vibrational states with less internal energy than the narrow detection at small λ_{fl}, which on average increases decay periods (slower dynamics) observed at large λ_{fl}, taking into account the incomplete solvent-induced vibrational relaxation (vibrational cooling process) of 2*S*-ABP occurring on the same time scale as for AB in solutions (10−20 ps).[4,14,33] Furthermore, the shape of the S_1 PES should be considered for the observed fluorescence wavelength dependency. As the rotational channel is blocked in 2*S*-ABP, the S_0–S_1 energy gap of the molecule is expected to decrease continuously along the concerted inversion reaction path all the way from the FC region to the S_0–S_1 surface-crossing area (Scheme 1). Because detection at small λ_{fl} is more sensitive to emission occurring at smaller intervals when the S_0–S_1 energy gap is larger, the

Femtosecond Dynamics of Azobenzenophanes

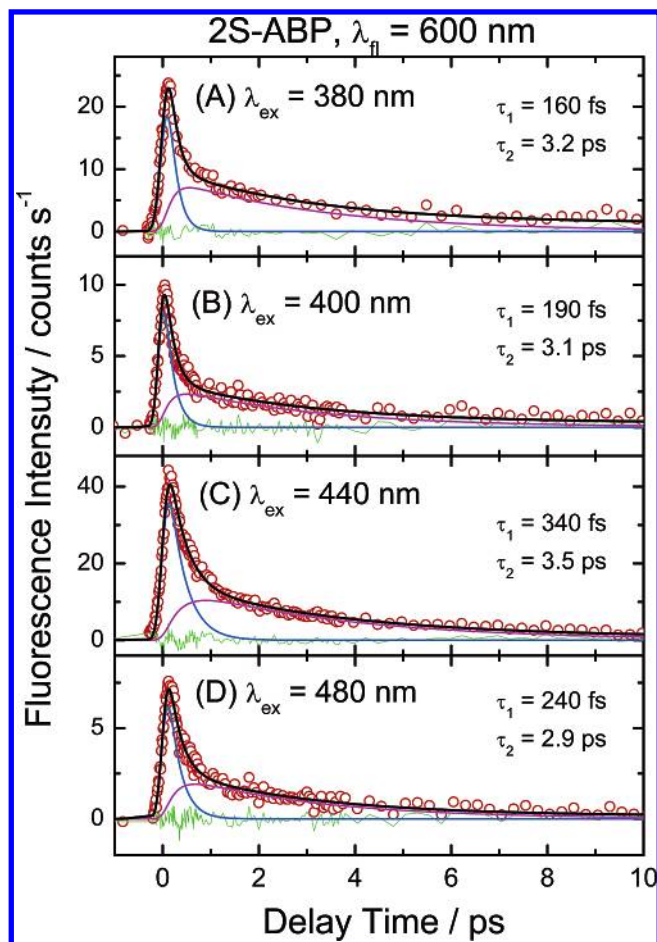*J. Phys. Chem. A, Vol. 109, No. 10, 2005* **2095**

Figure 4. Femtosecond fluorescence transients of 2*S*-ABP probed at a common detection window (λ_{fl} = 600 nm) but excited at wavelengths λ_{ex} (nm) = (A) 380, (B) 400, (C) 440, and (D) 480. Colors are the same as in Figure 3.

Figure 5. Femtosecond fluorescence transients of 2*S*-ABP obtained at λ_{ex} = 360 nm with fluorescence probed at λ_{fl} (nm) = (A) 450, (B) 500, and (C) 550. The transients in parts B and C contain small offset signals represented by the cyan curves. All other colors are the same as in Figure 3.

emission might become nonresonant at a greater delay when the S_0–S_1 energy gap becomes too small to be detectable. As a result, the detection window resulting from $S_1 \rightarrow S_0$ emission is narrower at small fluorescence wavelengths than the detection window at large fluorescence wavelengths, which leads to observation of smaller decay coefficients (τ_1 and τ_2) for the former. The observed wavelength dependency in relative amplitudes of the two components is also due to the detection window of the fluorescence probe; the initial FC relaxation was probed at an early stage at which the S_0–S_1 energy gap is larger, but the ensuing $S_1 \rightarrow S_0$ electronic relaxation was probed in a later stage at which the S_0–S_1 energy gap is smaller. Therefore, the detection at small λ_{fl} would probe greater populations in the FC region (larger S_0–S_1 energy gap) than in the S_1 minimum area (smaller S_0–S_1 energy gap), leading to the relative amplitudes of the two components being observed.

3.1.3. Dependency on Excitation Wavelength. We investigated the dynamical effect on excitation energy in a broad region of excitation wavelength at the same probe window (λ_{fl} = 600 nm) of the $S_1 \rightarrow S_0$ fluorescence. The results shown in Figures 4A–D are the fluorescence transients obtained at λ_{ex} = 380, 400, 440, and 480 nm, respectively. In general, all transients show biexponential decays that are satisfactorily described according to the consecutive kinetic model, eqs 1–3. Moreover, excitation at other wavelengths in the $S_0 \rightarrow S_1$ absorption region shows that the decay of the slow component at a specific fluorescence wavelength is virtually independent of excitation wavelength. This indicates that the emission stems from the same respective areas
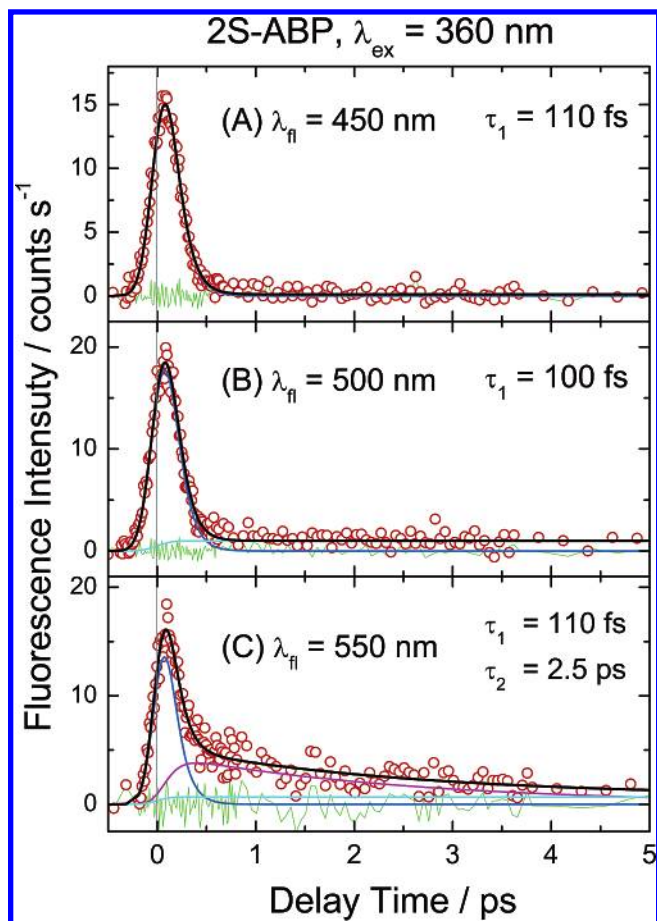
of the S_1 PES regardless of excitation energy. However, τ_1 increases as the excitation energy decreases, from 160 fs at λ_{ex} = 380 nm to 340 fs at λ_{ex} = 440 nm, then to 240 fs at λ_{ex} = 480 nm. Hence, the rate of the initial FC relaxation in 2*S*-ABP depends on the energy of the prepared FC state whereas the rate of searching for the S_0/S_1 CI on the S_1 PES is roughly independent of the energy at which the system is monitored. The opposite trend in τ_1 at λ_{ex} = 480 nm might reflect a vibronic coupling effect through the symmetric CNN bending motion as discussed for the case of AB.[26] Even though the observed greater rate of FC relaxation (τ_1^{-1}) at small λ_{ex} reflects a normal dynamical behavior of 2*S*-ABP moving along the concerted inversion coordinate on the S_1 surface (Scheme 1), the excitations at λ_{ex} = 380 and 400 nm may also prepare excited molecules in the S_2 state or the lower S_2–S_2 exciton coupling state (Figure 2). To study the S_2 dynamics of 2*S*-ABP, we performed experiments at a small excitation wavelength (λ_{ex} = 360 nm).

3.1.4. S_2 Dynamics. The dynamical behavior of 2*S*-ABP on S_2 excitation was investigated at λ_{ex} = 360 nm; the results are shown in Figures 5A–C with λ_{fl} = 450, 500, and 550 nm, respectively. The fluorescence transient observed at λ_{fl} = 450 nm, which can be attributed to $S_2 \rightarrow S_0$ fluorescence, shows predominantly a spikelike component with the decay coefficient being poorly evaluated (~100 fs) because of the limit of temporal resolution of the instrument (fwhm ~270 fs). In addition to the spikelike component shown in the transients, an ambiguous offset-like component was observed at λ_{fl} = 500 nm, which becomes more pronounced at λ_{fl} = 550 nm and

shows a decay feature with a time coefficient of ~2.5 ps. At λ_{fl} = 450 and 500 nm, the fluorescence is still predominantly of the $S_2 \rightarrow S_0$ character, but the slower decay might also be due to a "hot" $S_1 \rightarrow S_0$ emission. This proposal is based on the fact that on $S_0 \rightarrow S_1$ excitation the slow components in the decay times for all probing emission wavelengths are comparable; however, on 360 nm ($S_0 \rightarrow S_2$) excitation, the decay of the fluorescence probed at 550 nm is significantly slower than the decay on the $S_0 \rightarrow S_1$ excitation.

The above real-time observations indicate that there is only one process observed when the $S_2 \rightarrow S_0$ fluorescence is monitored, probably the ultrafast $S_2 \rightarrow S_1$ transition. At longer monitoring wavelengths, the emission contains contributions of the $S_1 \rightarrow S_0$ fluorescence, reflecting the dynamics of the S_1 PES after being populated from S_2. Thus, we conjecture that after excitation to the S_2 state a hot S_1 species is produced within 100 fs but the subsequent picosecond electronic relaxation on the S_1 PES might follow a path that has a different time characteristic than that of the relaxation of directly S_1 excited molecules and needs not necessarily end at the same place where the S_1 excited molecules are deactivated to the ground-state PES.

The above observations can be compared to those reported for femtosecond fluorescence dynamics of AB on S_2 excitation.[5,20] In the study of Fujino et al.,[20] $S_2 \rightarrow S_1$ relaxation of AB was observed to be ultrarapid (~110 fs) with a quantum yield almost unity. However, Schultz et al.[5] found two distinct relaxation time coefficients (170 and 420 fs) upon excitation of AB in a molecular beam at 330 nm; the fast- and slow-decay processes correspond to the S_2 and $S_{3,4}$ dynamics, respectively. According to recent theoretical calculations,[6] the lifetime of the S_3 state was found to be ~100 fs, and it is unlikely that the excited state of a very close lying pair could live for 420 fs. However, the observed ultrafast relaxation of the S_2 state is common for all measurements. The potential-energy diagrams of Cimicelli et al.[6] for AB show a S_1/S_2 CI at essentially the undistorted molecular geometry (FC-like structure), which rationalizes the ultrafast IC in AB and probably also in the ABPs. Semiclassical trajectory simulations[6] indicate that the symmetric CNN bending motion would even facilitate this electronic relaxation and a feasible motion along the concerted inversion channel can contribute to the observed ultrarapid kinetics of the $S_2 \rightarrow S_1$ relaxation. This dynamical feature is shown in Scheme 1.

The observation of an ultrarapid $S_2 \rightarrow S_1$ relaxation process in both AB and 2*S*-ABP invalidates the hypothesis of photoisomerization of AB occurring directly in the S_2 state. We have thus shown that photoisomerization of AB and 2*S*-ABP must occur in the lower-lying electronic states (either S_1 or S_0) regardless of initial excitation.

3.2. DMAB and 4*S*-ABP. Because the rotational channel in 2*S*-ABP is heavily restricted via chemical modification, electronic relaxation through the proposed concerted inversion channel becomes unique. To provide further experimental evidence for the proposed dynamical model (Scheme 1) and in an attempt to unravel the key issue for the enduring questions about the mechanism of photoisomerization of azobenzene, we have studied a rotation-free molecule with two methyl groups bound in the *para* positions (DMAB) and a rotation-blocked molecule with two AB moieties tightly connected via four thiaphane bridges (4*S*-ABP), with excitation at two wavelengths, namely, λ_{ex} = 360 and 430 nm.

3.2.1. S_2 Dynamics. Excitation with 360 nm radiation prepares the molecules in the S_2 state; the results are presented in Figure 6 and Table 2. Figures 6A− D compare the S_2 dynamics
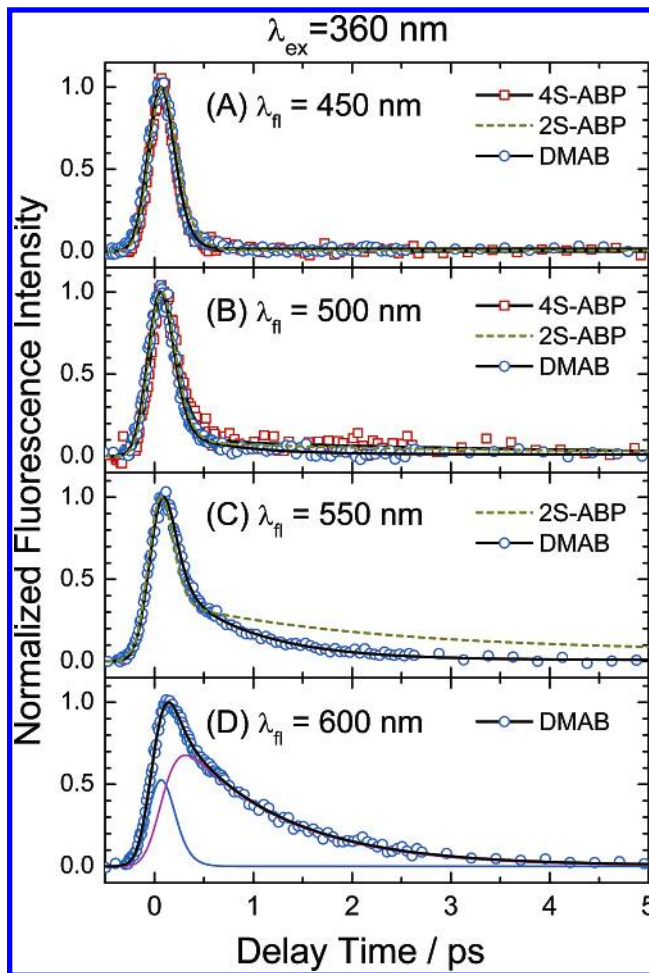
Figure 6. Femtosecond fluorescence transients of DMAB and 4*S*-ABP obtained at λ_{ex} = 360 nm with fluorescence probed at λ_{fl} (nm) = (A) 450, (B) 500, (C) 550, and (D) 600. The symbols denote raw data; corresponding black solid curves represent theoretical fits; the blue and magenta curves in part D are two deconvoluted components. The theoretical fits of 2*S*-ABP are shown as dark yellow dashed curves in parts A−C for comparison.

between DMAB, 2*S*-ABP, and 4*S*-ABP with detection at λ_{fl} = 450, 500, 550, and 600 nm, respectively. Similar to the case of 2*S*-ABP (theoretical fits are shown as dashed curves), the transients of DMAB and 4*S*-ABP probed at λ_{fl} = 450 nm (Figure 6A) show pulse-limited kinetics ($\tau_1 \approx 100$ fs), indicating that an ultrarapid $S_2 \rightarrow S_1$ transition is a fundamental feature for either the rotation-free or the rotation-restricted azobenzene derivative. At λ_{fl} = 500 nm (Figure 6B), a slow-decay component becomes just perceptible in all transients to reflect the following S_1 dynamics. At λ_{fl} = 550 nm (Figure 6C), the difference in the slow component of the transients between DMAB and 2*S*-ABP becomes more evident. At λ_{fl} = 600 nm (Figure 6D), the slow-decay component becomes a major part of the transient in DMAB. Because of the small solubility of the *S*-bridged compounds and the limit of detection sensitivity, fluorescence transients with an acceptable signal-to-noise ratio were not attainable for 2*S*-ABP at λ_{fl} = 600 nm and for 4*S*-ABP at λ_{fl} = 550 and 600 nm. Nevertheless, at λ_{fl} = 550 nm (Figure 6C), the observed time coefficient of the slow-decay component of DMAB ($\tau_2 = 0.9$ ps) is much smaller than that of 2*S*-ABP ($\tau_2 \approx 2.5$ ps), indicating the ensuing $S_1 \rightarrow S_0$ electronic relaxation to occur through different channels for DMAB and 2*S*-ABP.

3.2.2. S_1 Dynamics. Excitation with 430 nm radiation prepares the DMAB molecules in the S_1 state and the 4*S*-ABP molecules in the S_2 and S_1 states. The results are presented in Figure 7
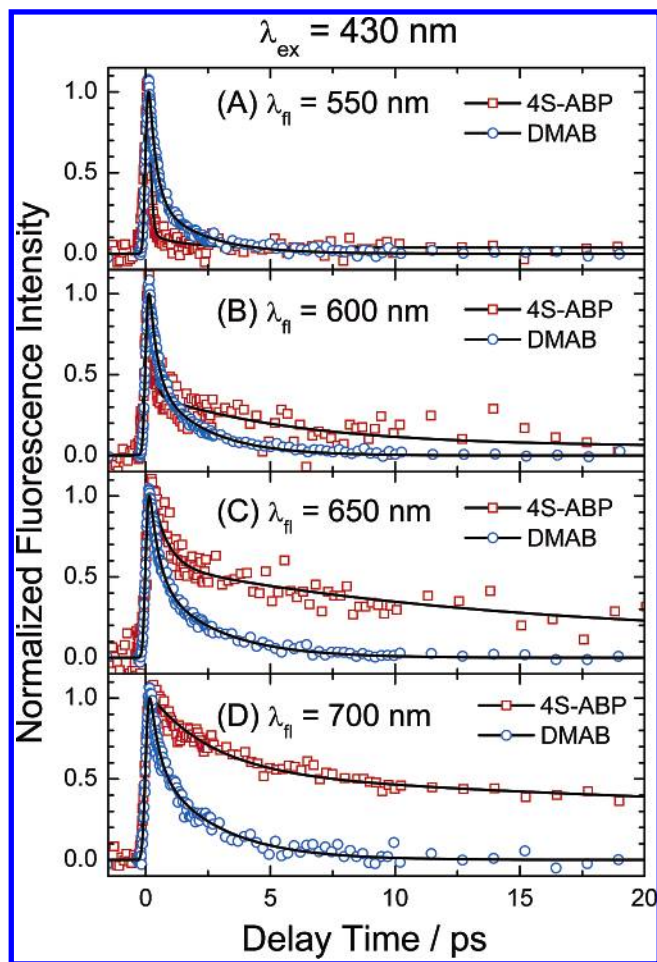
Figure 7. Femtosecond fluorescence transients of DMAB and 4*S*-ABP obtained at $\lambda_{\text{ex}} = 430$ nm with fluorescence probed at λ_{fl} (nm) = (A) 550, (B) 600, (C) 650, and (D) 700. The symbols denote raw data, with theoretical fits shown as black solid curves.

and Table 2. Figures 7A−D show the fluorescence transients of DMAB and 4*S*-ABP for $\lambda_{\text{fl}} = 550$, 600, 650, and 700 nm, respectively. The evident differences between the transients for DMAB and 4*S*-ABP are summarized in the following from three aspects. First, the slow-decay component of the transient of 4*S*-ABP at $\lambda_{\text{fl}} = 550$ nm is hardly observed. On close inspection, one realizes that 4*S*-ABP in contrast to DMAB has nearly no slow-decaying component, which might reflect the fact that S_2 in 4*S*-ABP is at lower energy than in DMAB (as shown in Figure 2). Therefore, at $\lambda_{\text{fl}} = 550$ nm predominantly $S_2 \rightarrow S_0$ is observed for 4*S*-ABP, but predominantly $S_1 \rightarrow S_0$ is observed for DMAB. This would again indicate the ultrafast IC of S_2 in 4*S*-ABP. Second, when the monitoring window is shifted to the $S_1 \rightarrow S_0$ fluorescence region, the slow component of 4*S*-ABP grows quickly at larger λ_{fl} and becomes appreciable at $\lambda_{\text{fl}} = 700$ nm. In contrast, the slow-decay components of the transients of DMAB in all probe windows show no such large change in relative amplitude. Third, both τ_1 and τ_2 of 4*S*-ABP increase greatly with increasing λ_{fl}, but in DMAB the variation of the time coefficients as a function of λ_{fl} is insignificant (Table 2). For example, τ_2 of DMAB increases by only 40% (from 1.8 ps at $\lambda_{\text{fl}} = 550$ nm to 2.5 ps at $\lambda_{\text{fl}} = 700$ nm) whereas τ_2 of 4*S*-ABP increases 40 times (from 1.3 to 56 ps) in the same range of λ_{fl}. In addition, a small offset (1−7%) was observed in the transients of 4*S*-ABP. These remarkable observations reflect the distinct topologies of the PES between DMAB and 4*S*-ABP and thus provide strong evidence for the $S_1 \rightarrow S_0$ electronic relaxation of DMAB being quite unlike that of 4*S*-

ABP. As both rotation and concerted inversion channels are accessible in DMAB but only the latter in 4*S*-ABP, we therefore suggest that opening of the rotational channel in DMAB is responsible for the observed S_1 dynamics in DMAB being much more rapid than those of 4*S*-ABP.

3.3. Comparison between AB/DMAB and 2*S*-ABP/4*S*-ABP. It now seems to be a relatively safe assumption that that the photoisomerization of azobenzene and its derivatives occurs on the S_1 surface and the isomerization mechanism can be rationalized from comparison of the observed $S_1 \rightarrow S_0$ relaxation dynamics between the rotation-free (AB or DMAB) and the rotation-restricted (2*S*-ABP or 4*S*-ABP) species. In the following, we highlight significant discrepancies in dynamics between molecules of the two types before stating a conclusion.

3.3.1. Key Differences in Dynamics between DMAB and 2S-ABP. The differences of relaxation dynamics observed between DMAB and 2*S*-ABP are summarized in three major points.

First, the rate of $S_1 \rightarrow S_0$ relaxation (τ_2^{-1}) is smaller for 2*S*-ABP than that for DMAB when observed at the same detection wavelength, e.g., (5.7 ps)$^{-1}$ versus (2.5 ps)$^{-1}$ at $\lambda_{\text{ex}} = 430$ nm and $\lambda_{\text{fl}} = 700$ nm. The observed much more rapid relaxation dynamics in DMAB than those in 2*S*-ABP are consistent with the selection of the rotational channel in DMAB. Hence, the $S_1 \rightarrow S_0$ deactivation via rotational motion should be considered to be a major relaxation channel in a rotation-free molecule like DMAB or AB.

Second, when the transient of 2*S*-ABP is observed at $\lambda_{\text{fl}} = 550$ nm, the value of τ_2 obtained on S_2 excitation ($\tau_2 = 2.5$ ps at $\lambda_{\text{ex}} = 360$ nm) is significantly larger than values of τ_2 obtained on S_1 excitations ($\tau_2 = 1.3$ and 1.4 ps at $\lambda_{\text{ex}} = 400$ and 440 nm, respectively); see Table 1. Such anomalous dynamical behaviors were not observed in DMAB and AB. Table 2 summarizes the results for DMAB; on S_2 excitation ($\lambda_{\text{ex}} = 360$ nm), τ_2 is 0.9 and 1.1 ps at $\lambda_{\text{fl}} = 550$ and 600 nm, respectively, which is smaller than on S_1 excitation ($\lambda_{\text{ex}} = 430$ nm) where τ_2 is 1.8 and 2.5 ps at the same fluorescence wavelengths. This normal dynamical trend is reported for another rotation-free species, AB, with $\tau_2 \approx 500$ fs[20] and 1−2 ps[26,28] on S_2 and S_1 excitations, respectively. The atypical dynamical trend observed in *2S*-ABP might be due to a specific shape of the S_1 PES at a place reached only by a S_2 excited molecule. This place is the starting point of a different decay trajectory than the one offered by direct S_1 excitation. The molecule then makes a long journey on the multidimensional PES from the S_1/S_2 CI to reach the "sloped" photochemical funnel region (S_0/S_1 CI). However, on direct S_1 excitation, the motion from the FC state to the S_0/S_1 CI area is quicker; the involvement of a stronger vibronic coupling effect on direct S_1 excitation might also be considered.[26] In contrast, the normal dynamical trend observed in both AB and DMAB is consistent with a downward motion on the S_1 PES toward the energy-favorable photochemical funnel along the rotational pathway. Therefore, this experimental evidence indicates strongly that the mechanism of the photoisomerization mechanism differs between DMAB and 2*S*-ABP.

Third, the shape of the S_1 PES is expected to be strongly correlated to the observed S_1 relaxation dynamics at various fluorescence wavelengths; this feature has been examined on direct S_1 excitation with detection in a broad range of λ_{fl}. When we compare the results between 2*S*-ABP and DMAB on S_1 excitation (Tables 1 and 2), we find that τ_2 in 2*S*-ABP increased substantially from 1.4 ps at $\lambda_{\text{fl}} = 550$ nm to 6.0 ps at $\lambda_{\text{fl}} = 700$ nm, but τ_2 in DMAB increased only slightly from 1.8 ps at $\lambda_{\text{fl}} = 550$ nm to 2.5 ps at $\lambda_{\text{fl}} = 700$ nm. Moreover, the corresponding relative amplitude of the τ_2 component tripled
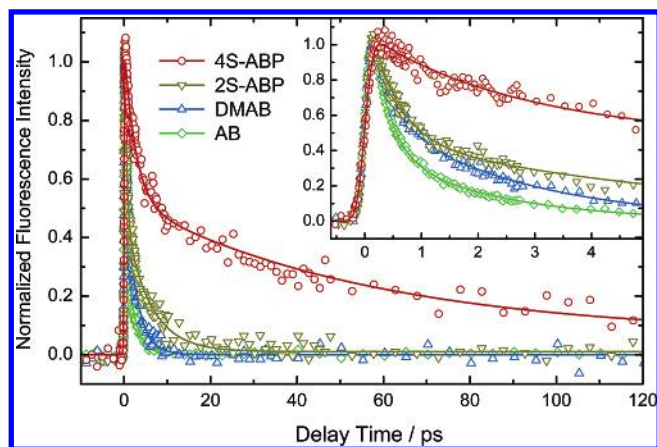
Figure 8. Comparison of femtosecond fluorescence transients between rotation-restricted (4S-ABP and 2S-ABP) and rotation-free (DMAB and AB) species obtained from the present study at λ_{ex} = 430 nm and λ_{fl} = 700 nm. The fitted time coefficients of 2S-ABP and DMAB/4S-ABP are listed in Tables 1 and 2, respectively; for AB, τ_1 = 290 fs and τ_2 = 1.9 ps. An inset compares the transients in the short time region.

in 2S-ABP from λ_{fl} = 550 nm to 700 nm, but the increment was only 60% in DMAB in the same detection window. These observations indicate that the motions of DMAB and 2S-ABP occur on excited-state surfaces with disparate topology. For example, the shape of the S_1 PES in DMAB might be much flatter than that in 2S-ABP so that a smaller variation of lifetimes and relative amplitudes was observed for the former. This inference is consistent with the topological picture obtained from theoretical calculations of AB; the S_1 PES of AB is practically flat along the rotation channel, but the energy and shape varies significantly for the S_1 surface along the concerted inversion channel.[7] Therefore, our results not only provide strong evidence for the mechanism of photoisomerization being distinct between DMAB and 2S-ABP but also support the isomerization of the molecule on the S_1 PES to occur via the rotation and the concerted inversion channels for DMAB and 2S-ABP, respectively.

3.3.2. Dynamical Effect on Molecular Rigidity. Figure 8 compares the S_1 dynamics of all four species, AB, DMAB, 2S-ABP, and 4S-ABP in nonviscous solvents, with excitation at λ_{ex} = 430 nm and detection at λ_{fl} = 700 nm. We observed a systematic variation of time coefficients in terms of molecular rigidity; τ_2 increases only slightly from 1.9 ps in AB to 2.5 ps in DMAB but substantially to 5.7 ps in 2S-ABP and greatly to 56 ps in 4S-ABP. The increase of τ_2 by 30% when the structure changes from AB to DMAB is understandable to reflect the effect of methyl substitutions in the *para* positions of the benzene rings of AB, which to some extent slows the motion of the phenyl groups along the rotation channel. A substantially decreased rate of relaxation is observed when the rotation channel is structurally restricted in 2S-ABP and 4S-ABP; in comparison to AB, the relaxation rate becomes smaller by factors of 3 and 30 for the former and the latter, respectively. It is remarkable that the rate of $S_1 \rightarrow S_0$ electronic relaxation of 4S-ABP is one tenth that of 2S-ABP. This observation is consistent with the nature of molecular rigidity for a much smaller rate of relaxation observed for a more rigid structure. Because the benzene rings are bound at 1,4-positions in 2S-ABP but are tightly locked at 1,3,5-positions in 4S-ABP, we expect the twisting motion along the CN single bond to play an important role in the observed S_1 dynamics. The above observation might also indicate that along the concerted inversion channel (Scheme 1) the location of the S_0/S_1 CI is

energetically much higher in 4S-ABP than in 2S-ABP. Further theoretical calculations might elucidate the observed dynamical behavior between 2S-ABP and 4S-ABP.

4. Concluding Remarks

Additional experimental evidence for the photoisomerization mechanism of *trans*-azobenzene is provided through comparison of the femtosecond fluorescence dynamics between the rotation-restricted azobenzenophanes (2S-ABP and 4S-ABP) and the rotation-free azobenzene derivative (DMAB) in nonviscous solvents on both S_1 and S_2 excitations.

With excitation to the S_2 state, we observed ultrarapid kinetics for the $S_2 \rightarrow S_1$ electronic relaxation for all three molecules, consistent with previous femtosecond results by Tahara and co-workers[4,20] that the observed $S_2 \rightarrow S_1$ quantum yield is near unity. This observation indicates the *trans* $\rightarrow$ *cis* photoisomerization of azobenzene occurs in a lower-lying electronic state (either S_1 or S_0) regardless of initial excitation into either the S_2 or S_1 state and thus adds weight to the argument against Rau's hypothesis of a rotation mechanism of isomerization in the $S_2(\pi,\pi^*)$ state.

With excitation to the S_1 state, we observed a substantial difference of relaxation rates between DMAB where rotation is possible and 2S-ABP/4S-ABP where rotation is restricted or blocked. Calculations agree in that the rotation-free molecules deactivate via a conical intersection near the 90° twist geometry.[6,7,22-24] Indeed, the $S_1 \rightarrow S_0$ relaxation rate of DMAB in a nonviscous solvent is far greater than that of the rotation-restricted azobenzenophanes. The geometrical constraint in these molecules should lead to a lifting up of the S_1 PES along the rotational coordinate, rendering the conical intersection near the 90° twist geometry inaccessible for rotation-restricted molecules. Then the $S_1 \rightarrow S_0$ electronic relaxation in both 2S-ABP and 4S-ABP molecules might occur through a conical intersection on the concerted inversion coordinate according to calculations of AB,[7] which however is at higher energy. The calculations of Ciminelli et al.[6] and of Cembran et al.[24] for AB suggest that the trajectories are neither pure rotation nor pure inversion and the great discrepancy of relaxation rates observed between 2S-ABP and 4S-ABP reflects the significance of molecular rigidity on the topology of the excited-state potential-energy surface, affecting the corresponding relaxation dynamics.

This work does not contradict Rau's hypothesis of a dual rotation/inversion mechanism in the photoisomerization of azobenzenes, but it rejects the neat separation of the two mechanisms in two separate states. Persico and co-workers[6] have shown by calculations that the enigmatic quantum yield data can be explained by the difference in the dynamics of deactivation for molecules prepared at different loci of the S_1 PES either by direct excitation or by internal conversion from S_2. Unfortunately, this experimental work cannot contribute to verification of this new concept.

References and Notes

(1) *Photoreactive Organic Thin Films*; Sekkat, Z., Knoll, W., Eds.; Academic Press: Amsterdam, 2002, and references therein.

(2) Rau, H. In *Photochromism: Molecules and Systems*; Durr, H., Bouas-Laurent, H., Eds.; Elsevier: Amsterdam, 1990, pp 165−192, and references therein.

(3) Tamai, N.; Miyasaka, H. *Chem. Rev.* **2000**, *100*, 1875−1890.

(4) Fujino, T.; Arzhantsev, S. Y.; Tahara, T. *Bull. Chem. Soc. Jpn.* **2002**, *75*, 1031−1040.

(5) Schultz, T.; Quenneville, J.; Levine, B.; Toniolo, A.; Martinez, T. J.; Lochbrunner, S.; Schmitt, M.; Shaffer, J. P.; Zgierski, M. Z.; Stolow, A. *J. Am. Chem. Soc.* **2003**, *125*, 8098−8099.

(6) Ciminelli, C.; Granucci, G.; Persico, M. *Chem.—Eur. J.* **2004**, *10*, 2327−2341.

(7) Diau, E. W.-G. *J. Phys. Chem. A* **2004**, *108*, 950−956.

(8) Rau, H.; Lüddecke, E. *J. Am. Chem. Soc.* **1982**, *104*, 1616−1620.

(9) Rau, H. *J. Photochem.* **1984**, *26*, 221−225.

(10) Rau, H.; Shen, Y.-Q. *J. Photochem. Photobiol., A* **1988**, *26*, 221−225.

(11) Röttger, D.; Rau, H. *J. Photochem. Photobiol., A* **1996**, *101*, 205−214.

(12) Monti, S.; Orlandi, G.; Palmieri, P. *Chem. Phys.* **1982**, *71*, 87−99.

(13) Lednev, I. K.; Ye, T.-Q.; Hester, R. E.; Moore, J. N. *J. Phys. Chem.* **1996**, *100*, 13338−13341.

(14) Nägele, T.; Hoche, R.; Zinth, W.; Wachtveitl, J. *Chem. Phys. Lett.* **1997**, *272*, 489−495.

(15) Lednev, I. K.; Ye, T.-Q.; Matousek, P.; Towrie, M.; Foggi, P.; Neuwahl, F. V. R.; Umapathy, S.; Hester, R. E.; Moore, J. N. *Chem. Phys. Lett.* **1998**, *290*, 68−74.

(16) Lednev, I. K.; Ye, T.-Q.; Abbott, L. C.; Hester, R. E.; Moore, J. N. *J. Phys. Chem. A* **1998**, *102*, 9161−9166.

(17) Hirose, Y.; Yui, H.; Sawada, T. *J. Phys. Chem. A* **2002**, *106*, 3067−3071.

(18) Satzger, H.; Root, C.; Braun, M. *J. Phys. Chem. A* **2004**, *108*, 6265−6271.

(19) Fujino, T.; Tahara, T. *J. Phys. Chem. A* **2000**, *104*, 4203−4210.

(20) Fujino, T.; Arzhantsev, S. Y.; Tahara, T. *J. Phys. Chem. A* **2001**, *105*, 8123−8129.

(21) Cattaneo, P.; Persico, M. *Phys. Chem. Chem. Phys.* **1999**, *1*, 4739−4743.

(22) Ishikawa, T.; Noro, T.; Shoda, T. *J. Chem. Phys.* **2001**, *115*, 7503−7512.

(23) Diau, E. W.-G.; Zewail, A. H. *Chem. Phys. Chem.* **2003**, *4*, 445−456.

(24) Cembran, A.; Bernardi, F.; Garavelli, M.; Gagliardi, L.; Orlandi, G. *J. Am. Chem. Soc.* **2004**, *126*, 3234−3243.

(25) Malkin, S.; Fischer, E. *J. Phys. Chem.* **1962**, *66*, 2482−2486.

(26) Chang, C.-W.; Lu, Y.-C.; Wang, T.-T.; Diau, E. W.-G. *J. Am. Chem. Soc.* **2004**, *126*, 10109−10118.

(27) Satzger, H.; Sporlein, S.; Root, C.; Wachtveitl, J.; Zinth, W.; Gilch, P. *Chem. Phys. Lett.* **2003**, *372*, 216−223.

(28) Lu, Y.-C.; Chang, C.-W.; Diau, E. W.-G. *J. Chin. Chem. Soc.* **2002**, *49*, 693−701.

(29) Valeur, B. *Molecular Fluorescence*, Wiley-VCH: Weinheim, Germany, **2002**, Chapter 6, and other related references therein.

(30) Pedersen, S.; Zewail, A. H. *Mol. Phys.* **1996**, *89*, 1455−1502.

(31) We infer monodispersed molecules as the following three points: (i) the spectrum is very azobenzene-like, and earlier we have taken an NMR spectrum in CDCl$_3$ supersaturated solution from samples with a similar UV spectrum (Gräf, D.; Nitsch, H.; Ufermann, D.; Sawitzki, G.; Rau, H. *Angew. Chem., Intl. Ed. Engl.* **1982**, *24*, 313−314); (ii) azobenzene has not been observed to aggregate even at a concentration as high as 0.1 M according to our unpublished results; (iii) azobenzene has been observed to aggregate only when external forces are applied by integration of derivatives in supramolecular structures (e.g., Schinomura, M.; Kunitake, T. *J. Am. Chem. Soc.* **1987**, *109*, 5175−5183).

(32) For 2*S*-ABP and 4*S*-ABP, the absorption of the S$_2$ state (and the possible "S$_2$−S$_2$ exciton coupling state") extends to about 450 nm as determined by extrapolation of the band head. So excitation with 360 nm irradiation prepares only the S$_2$ molecules, excitation with 480 nm prepares only the S$_1$ molecules, and excitation at 380, 400, and 440 nm prepares molecules in S$_2$ and molecules in S$_1$. On the basis of the fluorescence spectrum given by Fujino et al.[4] and considering the shift between AB and the other compounds (Figure 2), we locate the S$_2 \rightarrow$ S$_0$ emission between 400 and 550 nm and the S$_1 \rightarrow$ S$_0$ emission at wavelengths longer than 550 nm. One should be aware that by selecting different wavelengths for the fluorescence analysis one probes a different locus on the PES of the upper state.

(33) Hamm, P.; Ohline, S. M.; Zinth, W. *J. Chem. Phys.* **1997**, *106*, 519−529.